Research Article Vol. 10, No. 8 | 1 Aug 2019 | BIOMEDICAL OPTICS EXPRESS 3875

Biomedical Optics EXPRESS

Identifying crossing collagen fibers in human corneal tissues using pSHG images

M. ALIZADEH,[1,2,7] D. MERINO,[2,3,7] G. LOMBARDO,[4,5] M. LOMBARDO,[5] R. MENCUCCI,[6] M. GHOTBI,[1] AND P. LOZA-ALVAREZ[2,*]

[1] *Department of Physics, University of Kurdistan, Pasdaran St., 66177-15177, Sanandaj, Iran*
[2] *ICFO-Institut de Ciencies Fotoniques, The Barcelona Institute of Science and Technology, Castelldefels, 08860, Barcelona, Spain*
[3] *UOC, Universitat Oberta de Catalunya, Barcelona, 08018, Barcelona, Spain*
[4] *CNR-IPCF, Istituto per i Processi Chimico-Fisici, Viale F. Stagno D'Alcontres 37, 98158, Messina, (Italy)*
[5] *Vision Engineering Italy srl, Via Livenza 3, 00198 Rome, Italy*
[6] *Eye Clinic, Department of Surgery and Translational Medicine, University of Florence, 50121, Florence, Italy*
[7] *Authors contributed equally to this paper.*
**pablo.loza@icfo.eu*

Abstract: Polarization sensitive second harmonic generation (pSHG) microscopy has been used previously to characterize the structure of collagen fibers in corneal samples. Due to the typical organization of the corneal stroma, the information that pSHG provides may be misleading in points where two different collagen fiber bundles orient along different direction crossings. Here, a simulation that illustrates the problem is presented, along with a novel method that is capable of identifying these crossing points. These results can be used to improve the evaluation of corneal collagen structure, and it has been applied to analyze pSHG data acquired from healthy and keratoconic human corneal samples.

1. Introduction

The shape and transparency of the optical media of the eye, like the cornea or the crystalline lens, play an important role in the quality of image formation on the retina. The microscopic structure of these biological tissues is closely related to their optomechanical characteristics. In the case of cornea, its shape and transparency are provided by this structure. The corneal stroma is formed by a number of stacked lamellae of type I collagen fibrils, although type VI collagen and proteoglycans can also be found in its structure [1–4]. Any alteration of this structure, caused by either trauma or disease, can lead to changes in the physical and optical characteristics of the cornea, and result in vision loss [2].

Different techniques have been used to characterize the microstructure of the human cornea in the past. X-ray microscopy and scanning electron microscopy have been proposed to precisely characterize molecular structure of the corneal collagen, such as the calculation of its helical pitch angle [2,4,5]. However, these techniques require sample preparation protocols that are not compatible with *in vivo* measurements. Recently, multiphoton (MP) microscopy has been used to study the microscopic structure of different types of biological tissue, including human corneal samples. MP microscopy has a great potential for *in vivo* studies due to the following three main reasons: firstly, different molecules present in a biological tissue can be observed by means of MP microscopy without the requirement of any exogenous contrast agents [6]. Secondly, MP signal is usually generated by means of ultrashort laser pulses at intensity values that are safe for *in vivo* experiments. Furthermore, the applied excitation wavelength is usually close to the infrared, and exhibits high tissue penetration. Thirdly, MP microscopy features intrinsic axial depth discrimination and reduced photodamage.

#368459 https://doi.org/10.1364/BOE.10.003875
Journal © 2019 Received 29 May 2019; accepted 17 Jun 2019; published 10 Jul 2019

From all of the different MP microscopy techniques, second harmonic generation (SHG) microscopy has become very popular for studies of the cornea. This is due to the fact that corneal collagen is packed in the tissue in such a way that it behaves like an SHG active polycrystalline lattice [7–10]. This characteristic has been used in the past to observe the orientation of the collagen fibers using different theoretical models [9,11–15]. In particular, the application of polarization sensitive SHG (pSHG) has been reported for the classification of human corneal images according to the depth in the tissue at which they were acquired [16]. In these experiments, the polarization direction of the excitation beam is changed, resulting in a modulation in the intensity of the SHG signal obtained from the tissue. This modulation is related to the angle between the polarization of the excitation beam and the orientation of SHG active molecules. However, in this model it is assumed that all of the SHG active molecules within a pixel volume, or voxel, are oriented along the same direction. This requirement can produce misleading results in the study of corneal collagen tissue, since the corneal collagen fibers usually intertwine and are oriented along different directions. This situation is found especially in the anterior portion of the stroma, which plays the most important role in bearing stress and maintaining corneal shape [3,14–16].

In this work, the effects that collagen fiber crossings can have on the results of the pSHG model are illustrated. A method that is aimed at improving the information that can be generated by means of this pSHG biophysical model is also presented. This method is able to detect the pixels of the pSHG images that include the contribution of bundles of collagen fibers oriented along different directions. Once these pixels are detected, they can be filtered out, providing more reliable information related to the orientation and molecular structure of the collagen fiber bundles. These results have been experimentally tested on starch samples and also on healthy and keratoconic corneas.

2. Materials and methods

2.1. Biophysical model

The biophysical model used in this work has been described extensively in previous studies [17–22]. This model can predict the intensity of SHG signal, I_{SHG}, generated by an active supramolecular assembly with cylindrical symmetry depending on the excitation beam polarization orientation, α, and also the orientation of the SHG active molecule, φ, as follows [17]:

$$I_{SHG}(\varphi,\alpha) = a_0 + a_2 \cos 2(\varphi-\alpha) + a_4 \cos 4(\varphi-\alpha), \tag{1}$$

where a_0, a_2 and a_4 are coefficients that will be described in more detail in the following paragraphs. By taking the Fourier Transform (FT) of Eq. (1) with respect to α the following expression is reached [11]:

$$i(\varphi,\Omega) = a_0\delta(0) + a_2 \exp(i2\varphi)\delta(1-\Omega) + a_4 \exp(i4\varphi)\delta(2-\Omega) + c.c., \tag{2}$$

where Ω is the spatial frequency in the Fourier domain, and c.c. indicates the complex conjugate.

From Eq. (2), it is possible to calculate two different quantities related to the molecular structure of the SHG active assembly: the orientation of the supramolecular assembly, φ, and the orientation of the hyperpolarizability tensor dominant axis, θ_e. In the case of corneal collagen, φ is usually related to the orientation of the collagen fiber bundles, and θ_e has been previously related to the helical pitch angle of the collagen triple helix. These identifications will be assumed from now on in this text. However, the general meaning of φ and θ_e should be considered when extending this model to other types of tissue.

The helical pitch angle, θ_e, can be calculated from the parameters in Eq. (2) as follows [11]:

$$\tan^2\theta_e = \frac{2}{\sqrt{\dfrac{a_0 + a_2 + a_4}{a_0 - a_2 + a_4}}}. \tag{3}$$

In the case of the orientation of the collagen fibers, φ, it can be determined by computing the complex argument of the second coefficient in Eq. (2) as:

$$\varphi = \arg[a_2 \exp(i2\varphi)]/2. \tag{4}$$

At this point, it is worth noting that, according to Eq. (2), the same information can also be extracted from the third component in that equation:

$$\varphi = \arg[a_4 \exp(i4\varphi)]/4. \tag{5}$$

It has also been detailed in previous studies that the values of the coefficients a_0, a_2 and a_4 can be calculated from θ_e, [11,23], and their explicit expressions are:

$$a_0 = \frac{A^2}{8}\left[\frac{12}{\tan^4(\theta_e)} + \frac{4}{\tan^2(\theta_e)} + 7\right], \tag{6}$$

$$a_2 = \frac{A^2}{2}\left[\frac{4}{\tan^4(\theta_e)} - 1\right], \tag{7}$$

$$a_4 = \frac{A^2}{8}\left[\frac{4}{\tan^4(\theta_e)} - \frac{4}{\tan^2(\theta_e)} - 3\right]. \tag{8}$$

Note that A is a proportionality constant that appears in all of the components and here it will be set to 1, since it won't affect the calculations in Eqs. (3), (4) or (5).

According to this, for any given value of φ and θ_e, the intensity of the SHG signal can be determined for a particular value of α using Eq. (1). However, the described model assumes that the orientation of the SHG active molecules is well defined, and therefore all the molecules are oriented in a particular direction. As already mentioned, this may not be accurate for collagen fibers in different lamellae of the cornea.

Previous reports have shown that the overall SHG intensity at a pixel where two collagen fiber bundles cross can be described as the sum of the signals generated by each of the isolated fibers [14,15]. This can be expressed as:

$$I_{TOT}(\alpha) = I_{SHG,1} + I_{SHG,2} = I_{SHG}(\alpha,\varphi_1) + I_{SHG}(\alpha,\varphi_2), \tag{9}$$

where $I_{TOT}(\alpha)$ is the total SHG signal intensity generated at a particular point in the sample, illuminated by a laser beam polarized along the direction α, while $I_{SHG,1}$ and $I_{SHG,2}$ are the SHG intensities generated on the fibers 1 and 2 respectively when considered independently.

To evaluate the error incurred by the pSHG model used when collagen fibers oriented along different directions are considered to be aligned along one specific and well-defined direction, we generated a set of numeric data. Two different matrices with 512x512 elements were generated, each matrix representing the orientation of a collagen fiber, φ, on each pixel. These matrices are shown in Fig. 1. The values of φ_1, showing the orientations of collagen fiber 1 from the first matrix relative to the horizontal axis, are shown in Fig. 1(a). The value of φ_1 changes between −90° and 90°. The second matrix with the values of φ_2, is shown in Fig. 1(b). It has been divided into two halves: in the left half, φ_2 was kept constant at a value of 0°, while in the right half, the value of φ_2 was changed as the angle with the horizontal axis, in the same way as φ_1. The values of φ_1 and φ_2 have been used to calculate $I_{SHG,1}$ and $I_{SHG,2}$ respectively, in Eq. (9). For that, we chose a value of $\theta_e = 45°$ close to the existing data for collagen [13,18,24] and by applying this value in Eqs. (6), (7) and (8) the values for the coefficients $a_0 = 2.875$, $a_2 = 1.5$ and $a_4 = -0.375$ were calculated. Similar to the actual pSHG experiment, which will be described in following sections, nine different values of α (from 0° to 180° with steps of 20°) were used to calculate $I_{SHG,1}$ and $I_{SHG,2}$ using Eq. (1). Finally, 9 different matrices of $I_{TOT}(\alpha)$ were calculated, one for each α value, as the sum of $I_{SHG,1}$ and $I_{SHG,2}$, according to Eq. (9). In this way, a simulation was designed to study the behavior of the pSHG model when two crossing collagen bundles are considered. A 3D set of $I_{TOT}(\alpha)$ data was generated with a resulting matrix of 512 × 512 × 9 elements. In this data set, it will be possible to differentiate two different situations: on the right half of the images the overall intensity will be the contribution of two collagen fiber bundles aligned in the same orientation, while on its left half the overall intensity will be the sum of the contributions of two fiber bundles oriented along different directions. Since φ_2 is kept constant on the left half of the image, while φ_1 is varying along the horizontal axis, all the possible angles between the two different sets of collagen fiber bundle orientations can be easily visualized in the result.

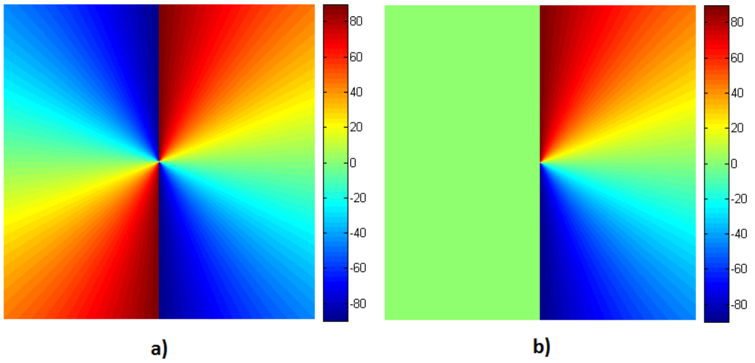

Fig. 1. The values of the orientation data for collagen fibers, a) φ_1 and b) φ_2, used as input to generate the theoretical data set of two crossing collagen fibers.

Once this theoretical data set was generated, the FT of $I_{TOT}(\alpha)$ was taken along the polarization direction, α, and Eqs. (3) and (4) were used to recover φ and θ_e [11]. The results of these calculations are shown in Fig. 2, and the recovered values will be referred to as φ_{res} and θ_{res} from this point on.

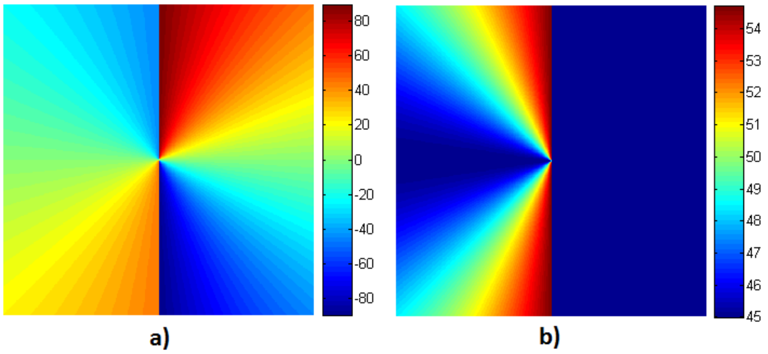

Fig. 2. The results of the pSHG model used with the theoretical data simulating two crossing collagen fibers generated as described. a) Values of φ_{res} and b) Values of θ_{res}.

In the case of φ_{res}, shown in Fig. 2(a), these values have been calculated using Eq. (4). As already explained, on the right half of the image, the results correspond to two collagen fiber bundles oriented along the same orientation, and this orientation is correctly recovered in φ_{res}. In the left half of the image, the results correspond to two collagen fibers oriented along different directions crossing. As it can be seen, on the horizontal line along the center of the image, the two collagen fiber bundles are oriented along the same axis. However, when the angle φ_1 is different to φ_2, the resulting value of φ_{res} becomes different from both φ_1 and φ_2. A similar situation occurs in Fig. 2(b), which shows the results for θ_{res}, calculated using Eq. (3) . As already mentioned, we used $\theta_e = 45°$ in Eq. (1), which corresponds to the result obtained in the right half of the image. However, on the left half, the contributions from the two fiber bundles with different orientations result in an increase in the value of θ_{res}, as the difference between φ_1 and φ_2 increases.

As explained previously, φ_{res} can be calculated in two different ways, using Eqs. (4) and (5). It should be noted that the *arg()* function returns values between ± 180°, therefore the resulting values of φ_{res} calculated from Eq. (4) will be phase wrapped between ± 90°, because φ is multiplied by a factor of 2 in the exponential function. This is consistent with the situation that is presented in this work, since the orientation of a fiber along 90° is equivalent to that of –90°.

Similarly, the value of φ_{res} calculated using Eq. (5) is phase wrapped between ± 45°, because the value of φ in the exponential term is multiplied by a factor of 4. For clarity, the values of φ_{res} calculated from the a_2 term in Eq. (4), are referred to as $\varphi_{res,2}$, while those calculated from the a_4 term in Eq. (5), are referred to as $\varphi_{res,4}$.

The values of $\varphi_{res,2}$ and $\varphi_{res,4}$ can be observed in Fig. 3(a) and (b), respectively. The figures show that the values of $\varphi_{res,4}$ present greater noise than those of $\varphi_{res,2}$. This can be explained by the fact that the a_4 component of the FT is usually much smaller than the one for a_2. In particular, in our simulation, the average value of the component a_2 in Eq. (2) over the whole image is 3.37, and for the component a_4 it is 1.36×10^{-15}. This last value is comparable to the accuracy of double type floating data in Matlab (which is in order of 10^{-16}), and hence the higher levels of noise in the results.

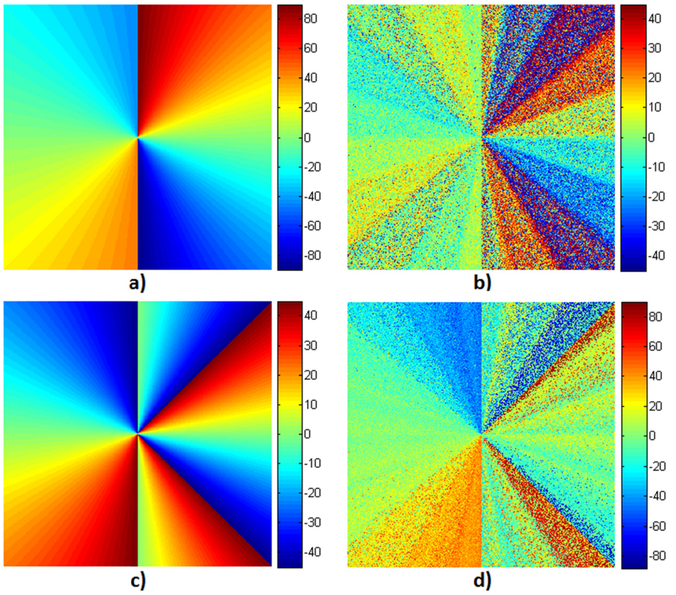

Fig. 3. The values of φ_{res} calculated by our simulation using a) Eq. (4), $\varphi_{res,2} = arg[a_2\exp(i2\phi)]/2$, and b) Eq. (5), $\varphi_{res,4} = arg[a_4\exp(i4\phi)]/4$. c) The values of $\varphi'_{res,2}$, calculated by phase wrapping the values of $\varphi_{res,2}$ between ± 45°. d) The values of $\Delta\varphi_{res} = (\varphi'_{res,2}-\varphi_{res,4})$.

At this point it is interesting to compare the values obtained for $\varphi_{res,2}$ and $\varphi_{res,4}$. Since $\varphi_{res,4}$ values range from –45° to 45°, it would seem necessary to unwrap them to values between –90° and 90°. However, this operation can be difficult, and it seems more convenient to phase wrap the values of $\varphi_{res,2}$ between ± 45° instead. The values of $\varphi_{res,2}$ wrapped between ± 45° will be referred to as $\varphi'_{res,2}$ from now on, and they are shown in Fig. 3(c). In order to show the similarity between $\varphi'_{res,2}$ and $\varphi_{res,4}$, the difference between these two quantities, which is called $\Delta\varphi_{res}$, was calculated and is shown in Fig. 3(d). It should be noted that the values of these results range from −90° to 90°, since the maximum difference between two quantities comprised between –45° and 45° can have an absolute value of 90°.

The results in Fig. 3(d) are interesting, and to better explain them, we have displayed them in a different way in Fig. 4. Figure 4(a) shows the data of $\Delta\varphi_{res}$ shown in Fig. 3(d), and in Fig. 4(b) the histogram Fig. 4(a) is presented. This histogram shows 5 different peaks: one peak around 0°, two peaks close to values of ± 90° and two more close to values of ± 45°. To understand what these peaks are related to, let us concentrate on the histograms of the left and right halves of the image separately.

Let's first consider the data of the right half of the image in Fig. 4(a). In this part of the image, all the molecules are oriented along the same direction, and it is expected that $\Delta\varphi_{res}$ would be close to zero. These are the data in Fig. 4(e). In the corresponding histogram, Fig. 4(f), it can be seen that the most repeated values for $\Delta\varphi_{res}$ are around 0°, which correspond to the pixels where the values of $\varphi'_{res,2}$ and $\varphi_{res,4}$ are very similar. However, there are also smaller peaks close to values of ± 90°. In the image, Fig. 4(e), the pixels with values of $\Delta\varphi_{res}$ close to ± 90° (these are the pixels in maroon and dark blue) are found along the directions ± 45°. These peaks come from the noise introduced by the calculation itself. To illustrate this, let us consider a point with $\varphi_{res,4} = 44°$, and assume that the noise changes the expected value of $\varphi_{res,4}$ by a 5% to a different amount of 46°. After phase wrapping, the new value of $\varphi_{res,4}$ would be –44°, which once subtracted from $\varphi'_{res,2}$ will produce a value of $\Delta\varphi_{res} = 88°$. As mentioned above, this situation will mainly arise around the values of φ close to the phase wrapping angle limit, which is indeed observed in Fig. 4(e).

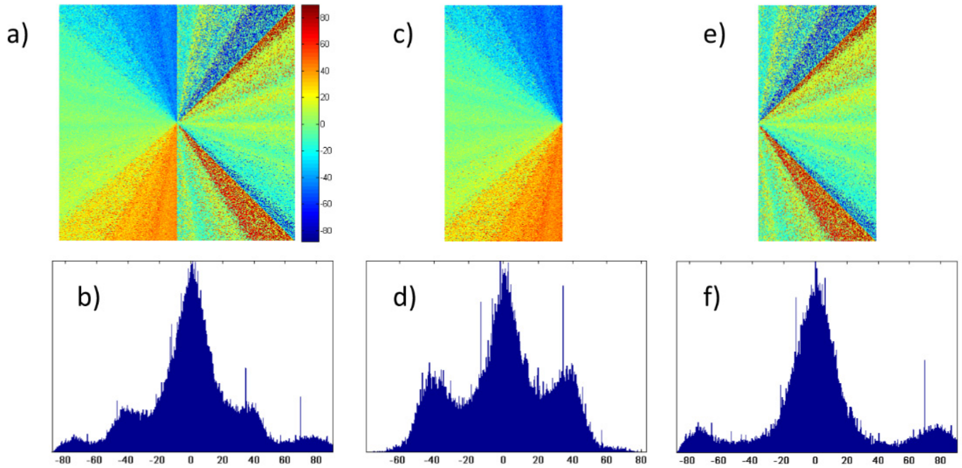

Fig. 4. a) Values of $\Delta\varphi_{res}$ identical to those in Fig. 3(d). b) Histogram of the values in a). c) Values of $\Delta\varphi_{res}$ only for the left-hand side (pixels with crossing fibers) of the data in a). d) Histogram of the values in c). e) Values of $\Delta\varphi_{res}$ only for the right-hand side (pixels with parallel fibers) of the data in a). f) Histogram of the values in e).

In Fig. 4(c), the results for the left half of the $\Delta\varphi_{res}$ image are shown. This data presents crossing collagen fibers along different directions. The largest values of $\Delta\varphi_{res}$ appear when the crossing fibers form angles of ± 90° (orange and blue pixels). In the corresponding histogram, Fig. 4(d), there is also a main peak around 0° as in the previous case. However, there are also peaks in $\Delta\varphi_{res}$ histogram around the values ~ ± 45°. These values correspond to the pixels where the two collagen fibers are not aligned and, they form a certain angle instead. In Fig. 4(c) it can be seen that these pixels correspond to those positions where the difference between the input values φ_1 and φ_2 is larger than 45°, which is where blue and orange pixels can be found.

After this consideration, it can be seen that the histogram in Fig. 4(b) shows all of the peaks described above: one large peak around 0°, two peaks at ± 90° and two more at ± 45°. Using the data in the histogram of Fig. 4(b) we can determine the pixels with crossing fibers, which would be those included in the peaks around ± 45°. These pixels have values of $\Delta\varphi_{res}$ in the ranges of (−53.11°, −22.92°) and (22.92°, 53.11°). This information can be used to identify and filter out the pixels with crossing fibers in order to obtain the collagen fiber orientations more reliably.

In the following sections, these results will be validated using the data acquired from different biological samples.

2.2 pSHG microscopy imaging

The results obtained with the simulation described in the previous section have been tested using the experimental data from real samples. To do this, the pSHG microscopy images have been acquired using a setup that has been fully described previously [13,21,23]. A Kerr lens modelocked Ti:sapphire laser (MIRA 900f, Coherent) was used as the excitation source. This pulsed laser source was operated at a central wavelength of 810 nm with a pulse duration of 160 fs (measured at the sample plane) and a repetition rate of 76 MHz. A water immersion 1.05 NA 25x objective (Plan Apochromat LWD*, Nikon) was applied to focus the light on the sample, while another 1.05 NA 25x water immersion objective (XLPlan N, Olympus) was used to collect the signal generated in the forward direction. The theoretical axial resolution of the system was 1 µm [25]. Typical frame acquisition time for a single 512x512 pixels image was about ~1.5 s. The effect of depolarization of the fundamental beam introduced by the different optical components was also measured at the sample plane, as previously described [13].

In a first approach, a starch granule was studied as a representative case for the pSHG model. It has been previously reported that the amylopectin molecules in a starch granule are SHG active, and that they are radially oriented within the granule, without any crossing between them [26]. The results obtained will be analyzed in detail in the following section.

Ex-vivo samples of healthy and keratoconic human corneas were also analyzed using our system and method. The samples were obtained in compliance with the guidelines of the Declaration of Helsinki for research involving the use of human tissue and the experimental protocol was approved by the local ethical committee (Clinic Barcelona, Hospital Universitari, Barcelona, Spain). The healthy corneas were provided by the Veneto Eye Bank Foundation (Zelarino Venezia, Italy) with the request of endothelial cell density ≥ 2000 cells/mm$^{2.}$ They were stored in 15% dextran-enriched corneal medium storage solution [16]. The corneas affected by keratoconus were harvested from patients undergoing penetrating keratoplasty at the Department of Ophthalmology of the University of Florence (Italy). Immediately after surgery, the corneas were immersed in 2.5% glutaraldehyde solution and shipped to the laboratory via express air courier for pSHG imaging.

For imaging, each corneal sample was placed in a custom-made chamber filled with 15% dextran. The sample was mounted on the microscope between two different #1 cover-slips (0.13 to 0.16 mm thick), with its anterior surface parallel to the scanning plane. Z-stacks of images of the whole depth of the sample were acquired. These images were taken at 5 µm intervals. Imaging was performed on several areas of the central 2 mm of each cornea. The optical power after the objective was measured to be ~15 mW and it was adjusted with imaging depth to compensate for signal attenuation. The power was increased up to 50% in deeper planes in order to cover the full dynamic range of the detector. We made sure that no damage occurred to the tissue during measurements; any alteration would have been observed clearly as a consequence of photodisruption [27].

Nine different pSHG images for each plane of focus were obtained by exciting the corneal lenticule with the same number of different linear polarizations [13,19]. Polarization of the excitation beam reaching the sample was changed using a rotating half wave plate. SHG images were obtained for the polarization values ranging from 0° to 180° at 20° steps. These images were stored for post-processing. In an attempt to reduce the noise in the images, each polarization experiment was repeated four times and then averaged. The overall acquisition time of a pSHG experiment was 1.5 minutes for each focal plane.

3. Results

In this section, the results obtained from the images of real samples are discussed. The section is divided into two parts: the analysis of the images of starch granules, and the same analysis for the excised corneal samples.

3.1 pSHG imaging of starch granules

Figure 5 shows some representative images of the pSHG images obtained from starch granules. Figure 5(a) shows the average of the 9 SHG intensity images with rotated polarizations acquired as described in the previous section. Figure 5(b) shows $\varphi_{res,2}$, the orientation of the pSHG active molecules in each pixel of the image, obtained using Eq. (4). A radial distribution is observed, as expected [26]. To test the validity of the model, $\Delta\varphi_{res}$ was also calculated for the sample. The pixels with $\Delta\varphi_{res}$ values laying between (−53.11°, −22.92°) and (22.92°, 53.11°) were identified. This information was used to generate a mask to reject these pixels from the data set, since the simulations show that these are the pixels with SHG active molecules oriented along different directions. The resulting image after these pixels were rejected is shown in Fig. 5(c). By comparing this image with the image in Fig. 5(b), it can be seen that only a few pixels of the data set are rejected. These rejected pixels correspond to molecules oriented close to $\varphi = \pm 45°$. As explained before, these are special values of φ because they are the limit angles for the phase wrapping of $\varphi_{res,4}$ values, where noise plays an important role. These results indicate that, except for the particular orientations $\varphi = \pm 45°$, our method is not affected by the orientation of the SHG active molecules. Figure 5(d) shows the histogram of θ_e values. These data have been fitted to a lognormal function. In the plot, θ_e values have been normalized to the peak value of the fitted curve. The mode of the fitted lognormal function, $\theta_e = 36.7°$, is in a good agreement with the values of the helical pitch angle for starch granules reported in previous works [24]. Since in this case very few points are rejected by the proposed analysis, these results for θ_e do not change considerably when using the described mask.

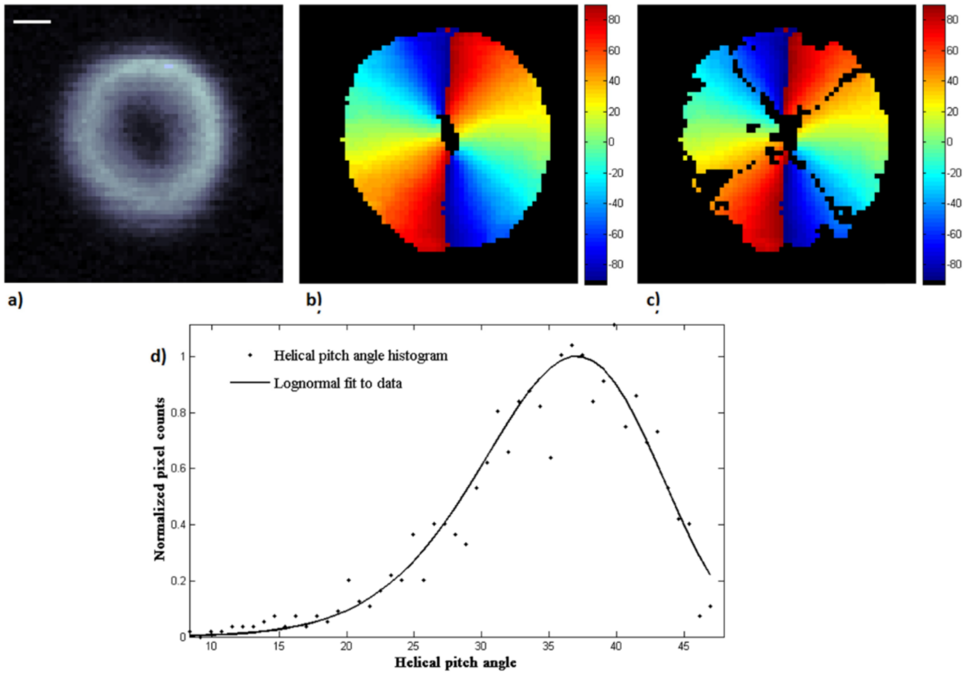

Fig. 5. a) Average intensity of the 9 pSHG images acquired from a starch granule. Scale bar is 10 µm. b) Values of $\varphi_{res,2}$ calculated from the image in a). c) The same image as in b) after applying a mask calculated using $\Delta\varphi_{res}$ as explained in the text. d) The histogram of θ_e values.

3.2 pSHG imaging of human corneal samples

As already mentioned, the use of the method described here has been extended to the study of the collagen fiber structure of healthy and keratoconic excised human corneal samples. Figure 6 shows some representative results, obtained from an excised healthy human cornea at a depth of 220 µm. Figure 6(a) shows the pSHG intensity image of the stroma calculated as the average of the pSHG images acquired for the 9 different polarization directions of the excitation beam, as described in section 2.2. In this image, the structure of the collagen fibers oriented along different directions can be clearly observed. Figure 6(b) shows the results of $\varphi_{res,2}$ obtained for this particular set of images using the pSHG model described in the previous studies. In these calculations, noisy pixels have been filtered out in a first approach by considering appropriate values for signal to noise ratio (SNR) of the SHG signal, and appear in black [16]. In the image, the collagen fibers appear in different colors, depending on their orientation calculated using the method described. The main components of the orientation of the fibers appear in the image in orange-yellow, which corresponds to the orientation angles of 25° to 35°. In addition, some dark blue fibers can be identified, corresponding to the angular range of –60° to –80°. These two main directional bands seem to be clearly represented in Fig. 6(a). However, the white circle in Fig. 6(b) shows some fibers in red, which correspond to the orientation of ~70°. Similarly, the red circle shows some fibers in green, which correspond to the orientation of ~0°. This image illustrates the problem that we discussed earlier, since these orientations do not correspond to those observed in Fig. 6(a).

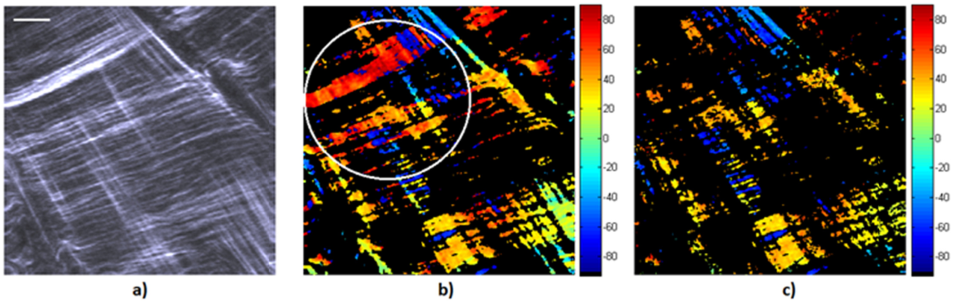

Fig. 6. pSHG data acquired from a normal cornea at a depth of 220 µm. a) Average intensity of the 9 pSHG images acquired. Scale bar is 10 µm. b) Collagen fiber orientations ($\varphi_{res,2}$) calculated using the pSHG model, Eq. (4). The circle highlights an area where the results of $\varphi_{res,2}$ do not correspond with apparent orientations of the fibers in a). In particular, in the white circle, a fiber in red (70°) appears to be aligned at around 30°-40°. Also, in the red circle, a fiber in green (0°) seems aligned along −70°. c) The same results as in b) after rejecting the pixels where crossing fibers have been identified, including these conflicting fibers.

Figure 6(c) shows the orientation data after the pixels with crossing fibers have been detected and filtered out using $\Delta\varphi_{res}$ information. As explained before, the values of $\Delta\varphi_{res}$ have been used to identify pixels with crossing fibers and mask them out. Visual inspection of the results shows that the red and green collagen fibers in Fig. 6(b) have been mostly removed from the data set after applying our method. However, the obtained collagen fiber orientations seem consistent with those shown in Fig. 6(a).

We have compared our results with those generated using methods based on the measurement of the SHG anisotropy parameter proposed in previous studies [14,15]. Figure 7(a) shows the pixels of the healthy cornea data set shown in Fig. 6 that have been identified as generated in a single collagen fiber using the SHG anisotropy parameter. In Fig. 7(b) the same result using our new method based on $\Delta\varphi_{res}$ measurement is shown. Figure 7(c) shows the pixels that have been identified only by one of the two methods. The number of pixels identified in Fig. 7(c) correspond to only ~4% of the pixels in the whole image.

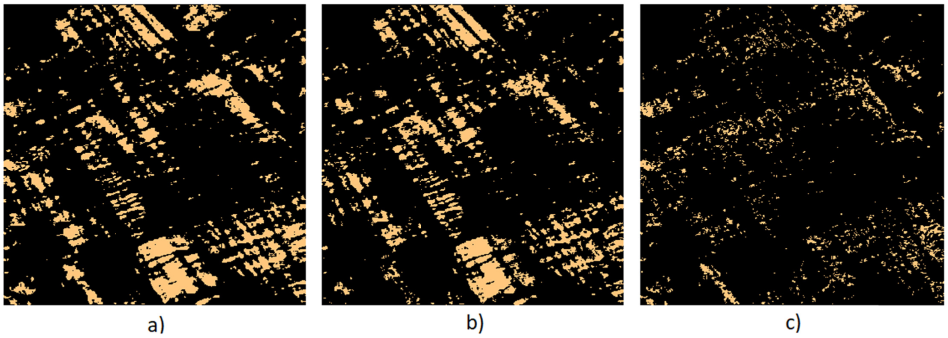

Fig. 7. Comparison of the pixels where pSHG signal has been identified as generated from a single collagen fiber using a) anisotropy parameter information, and b) our method based on $\Delta\varphi_{res}$ information. c) Pixels that have been identified by only one of the methods. This image is used as a way to determine the differences between the two methods.

As in the case of starch granules, the values of θ_e have also been calculated using the data from Fig. 6. These data were also masked using the results in Fig. 7(b) (similar to the procedure followed with φ detailed before). Figure 8(a) and b show the values of θ_e calculated before and after applying the mask. The histograms of the θ_e values in Fig. 8(a) and (b) are shown in Fig. 8(c). As in the case of the starch images, a lognormal function has been fitted to the data in order to estimate the peak value of the distribution. The number of pixels used for these two histograms is not the same, since the pixels where crossing fibers have been identified in Fig. 8(a) were rejected and not considered in Fig. 8(b). Therefore, for easier comparison of the two histograms, the data have been normalized to the peak of the fitted lognormal function, i.e. the values of the number of pixels for each θ_e value in the histogram have been divided by the maximum height of the fitted lognormal function. The results are shown in Fig. 8(c). The dashed and solid lines in the picture show the plot of the fitted curves of θ_e values in Fig. 8(a) and b respectively. The modes of these lognormal distributions are 48.1° when considering all pixels (Fig. 8(a)), and it is reduced to a value of 46.4° after rejecting pixels with crossing fibers (Fig. 8(b)). These values are compatible with previous experimentally measured reports of the helical pitch angle for collagen [13,18,24]. A shift of ~1.5° is observed in the modes of the fitted curves. This result is consistent with what was found in the simulation detailed in section 2.1, where one of the effects of crossing fibers in the pixels was the overestimation of θ_e value (Fig. 2(b)).

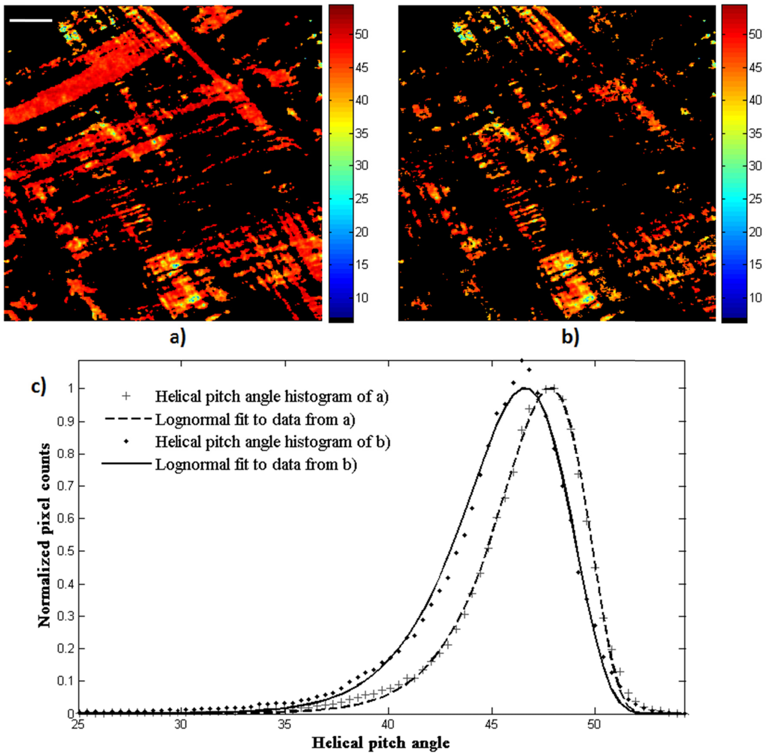

Fig. 8. Helical pitch angle of collagen fibers in normal cornea, a) before and b) after detecting and rejecting pixels with crossing fibers. Scale bar in a) is 10 µm. c) Helical pitch angle distribution and the resulting fit based on a lognormal function for the data in figures a) and b).

Data acquired from keratoconic corneas have also been studied using the method described in this article. Figure 9 shows some representative data for this sample. Figure 9(a) shows an average pSHG intensity image, where the characteristic collagen structure at a depth of 45 µm can be seen. The structure shown is similar to that in Fig. 6. Figure 9(b) shows the results of $\varphi_{res,2}$ obtained using the pSHG model described. The white circle in the image shows an area including alternating blue and red colored areas, corresponding to ~-70° and ~ + 70° approximately. However, in the SHG intensity image, Fig. 9(a), these fibers seem to be oriented along a direction of approximately –40°. Another interesting case corresponds to the fibers inside the red circle. The colors in these fibers indicate that they are oriented between angles from ~ + 20 to + 40°, while their orientations in the intensity picture seem to be closer to ~ + 75°. In Fig. 9(c), the pixels where crossing collagen fibers have been identified are rejected using the method described in this paper. The pixels with conflicting orientation values have been automatically identified and masked out. Visual inspection of the results show that the remaining collagen fiber orientations are consistent with the corresponding ones shown in Fig. 9(a). The values of θ_e have also been calculated. The modes of the lognormal distributions are 49.97° before rejecting the erroneous pixels and 49.39° after rejecting them. The shift in these values is ~0.6° for this image.

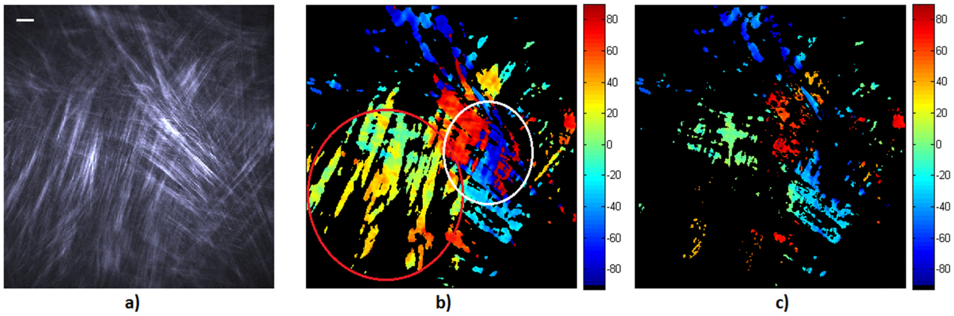

Fig. 9. pSHG data acquired from a keratoconic cornea at a depth of 45 μm. a) Average intensity of the 9 pSHG images acquired. Scale bar is 10 μm. b) Collagen fiber orientations ($\varphi_{res,2}$) calculated using the pSHG model. c) The same results as in b) after rejecting the pixels where crossing fibers have been identified.

These results illustrate that the method is effective to detect the pixels of pSHG images where collagen fiber bundles are crossing, both in the case of healthy and keratoconic corneas.

4. Discussion

In this work, a new method to analyze pSHG data acquired from images of excised human corneal tissues is presented. This model considers the possibility of different collagen fibers contributing to the overall pSHG image intensity in a single pixel. The method is based on a theoretical model that takes into account the variation of the pSHG intensity image with respect to the excitation beam polarization to calculate the orientation of collagen fibers. The main assumption for this model is that the overall pSHG signal in a pixel where two fibers with different orientations cross is the sum of the contribution from each of the two isolated fibers. The model has shown that failure to consider this effect can be a source of error in the estimation of the orientations of fibers containing the pSHG active molecules, and their helical pitch angle, which may be overestimated. The simulation has also provided an estimation for the values of the parameters, i.e. the range of $\Delta\varphi_{res}$ values, needed to evaluate the probability to have crossing fibers in a particular pixel of a pSHG image.

The newly developed model has been validated on starch granules. The results have confirmed that the pSHG active molecules in the starch granule are generally not oriented along different directions in the same pixel.

The primary interest was to apply the new model to the human cornea, and data has been acquired from ex-vivo healthy and keratoconic human corneal samples. The results obtained show that the model is able to automatically identify pixels of the image where crossing collagen fibers contribute to the overall pSHG signal. By masking these values, it has been possible to automatically discard pixels that showed orientation values that conflicted with visual observation. Also, after discarding these pixels, a shift toward lower values has been observed on the estimation of the helical pitch angle of the corneal collagen images. The results are in good agreement with the performed simulation, and have consistently provided values of θ_e that are compatible with the values reported in the bibliography [13,18,24].

It is worth noting here that using a system with higher axial resolution may be considered as a way to reduce the number of pixels with crossing fibers in pSHG images. However, this translates on a hardware configuration change to increase the numerical aperture of the objective used. This can be a limit to the performance of the system. Nevertheless, even with optimized axial resolution, misalignments between the image plane and the orientation of the lamellae in the cornea can occur, and this can lead to areas in the image including intersection between different lamellae and therefore the problem may still arise. In this sense, it seems appropriate to have a method that can determine the pixels that may detect conflicting results in an automated way.

We have therefore presented and tested a new method to determine the pixels in pSHG images which may contain information generated at different crossing collagen fibers, and the obtained results are in good agreement with similar methods available in the literature. The presented model has great potential in the study of the collagen structure in the human cornea, especially in its characterization to determine the differences between healthy corneas and those affected by disease known to have an impact on the collagen distribution, such as in the case of keratoconus. Future studies will aim at developing pSHG-based imaging biomarkers for identifying the number and density of crossing collagen fiber bundles in order to assess the structural integrity of cornea tissue.

Funding

University of Kurdistan, through the Iran Ministry of Science, Research and Technology; Spanish Ministry of Economy and Competitiveness and the "Severo Ochoa" program for Centres of Excellence in R&D (FIS2016-80455-R and SEV-2015-0522); UE: AEI/FEDER and H2020 LaserLab Europe (654148); Fundació Privada Cellex; Fundación Mig-Puig, Generalitat de Catalunya (CERCA program); "ROP EDFR 2014-2020 Lazio Innova" (A0114-2017-13715).

Acknowledgements

This research has been partially conducted at ICFO's Super Resolution Light Microscopy and Nanoscopy Facility. We thank Dr. David Artigas for his useful comments and invaluable help throughout the development of this work.

Disclosures

The authors declare that there are no conflicts of interest related to this article.

References

1. A. Daxer and P. Fratzl, "Collagen fibril orientation in the human corneal stroma and its implication in keratoconus," Invest. Ophthalmol. Vis. Sci. **38**(1), 121–129 (1997).
2. D. M. Maurice, "The structure and transparency of the cornea," J. Physiol. **136**(2), 263–286 (1957).
3. K. M. Meek and C. Knupp, "Corneal structure and transparency," Prog. Retin. Eye Res. **49**, 1–16 (2015).
4. K. M. Meek, S. J. Tuft, Y. Huang, P. S. Gill, S. Hayes, R. H. Newton, and A. J. Bron, "Changes in collagen orientation and distribution in keratoconus corneas," Invest. Ophthalmol. Vis. Sci. **46**(6), 1948–1956 (2005).
5. W. Radner, M. Zehetmayer, C. Skorpik, and R. Mallinger, "Altered organization of collagen in the apex of keratoconus corneas," Ophthalmic Res. **30**(5), 327–332 (1998).
6. S.-W. Chu, S.-Y. Chen, G.-W. Chern, T.-H. Tsai, Y.-C. Chen, B.-L. Lin, and C.-K. Sun, "Studies of $\chi(2)/\chi(3)$ Tensors in Submicron-Scaled Bio-Tissues by Polarization Harmonics Optical Microscopy," Biophys. J. **86**(6), 3914–3922 (2004).
7. H.-Y. Tan, Y. Sun, W. Lo, S.-J. Lin, C.-H. Hsiao, Y.-F. Chen, S. C.-M. Huang, W.-C. Lin, S.-H. Jee, H.-S. Yu, and C. Y. Dong, "Multiphoton fluorescence and second harmonic generation imaging of the structural alterations in keratoconus ex vivo," Invest. Ophthalmol. Vis. Sci. **47**(12), 5251–5259 (2006).
8. N. Morishige, A. J. Wahlert, M. C. Kenney, D. J. Brown, K. Kawamoto, T. Chikama, T. Nishida, and J. V. Jester, "Second-harmonic imaging microscopy of normal human and keratoconus cornea," Invest. Ophthalmol. Vis. Sci. **48**(3), 1087–1094 (2007).
9. W. Lo, W.-L. Chen, C.-M. Hsueh, A. A. Ghazaryan, S.-J. Chen, D. H.-K. Ma, C.-Y. Dong, and H.-Y. Tan, "Fast Fourier Transform-Based Analysis of Second-Harmonic Generation Image in Keratoconic Cornea2D-FFT Analysis of Structural Change in Keratoconic Cornea," Invest. Ophthalmol. Vis. Sci. **53**(7), 3501–3507 (2012).
10. R. Mercatelli, F. Ratto, F. Rossi, L. Menabuoni, A. Malandrini, F. Tatini, R. Nicoletti, R. Pini, F. S. Pavone, and R. Cicchi, "Three-dimensional mapping of corneal lamellar orientation by means of backward-scattered SHG

microscopy," in E. Beaurepaire, F. S. Pavone, and P. T. C. So, eds. Proceedings Volume **10414**, *Advances in Microscopic Imaging* (SPIE, 2017), p. 1041407.

11. I. Amat-Roldan, S. Psilodimitrakopoulos, P. Loza-Alvarez, and D. Artigas, "Fast image analysis in polarization SHG microscopy," Opt. Express **18**(16), 17209–17219 (2010).
12. C. Odin, T. Guilbert, A. Alkilani, O. P. Boryskina, V. Fleury, and Y. Le Grand, "Collagen and myosin characterization by orientation field second harmonic microscopy," Opt. Express **16**(20), 16151–16165 (2008).
13. P. Stoller, K. M. Reiser, P. M. Celliers, and A. M. Rubenchik, "Polarization-modulated second harmonic generation in collagen," Biophys. J. **82**(6), 3330–3342 (2002).
14. G. Latour, I. Gusachenko, L. Kowalczuk, I. Lamarre, and M.-C. Schanne-Klein, "In vivo multiphoton imaging of the cornea: polarization-resolved second harmonic generation from stromal collagen," in A. Periasamy, K. König, and P. T. C. So, eds. Proceedings Volume **8226**, *Multiphoton Microscopy in the Biomedical Sciences XII* (SPIE, 2012), p. 82262I.
15. G. Latour, I. Gusachenko, L. Kowalczuk, I. Lamarre, and M.-C. Schanne-Klein, "In vivo structural imaging of the cornea by polarization-resolved second harmonic microscopy," Biomed. Opt. Express **3**(1), 1–15 (2012).
16. M. Lombardo, D. Merino, P. Loza-Alvarez, and G. Lombardo, "Translational label-free nonlinear imaging biomarkers to classify the human corneal microstructure," Biomed. Opt. Express **6**(8), 2803–2818 (2015).
17. S. Psilodimitrakopoulos, S. I. Santos, I. Amat-Roldan, A. K. Thayil, D. Artigas, and P. Loza-Alvarez, "In vivo, pixel-resolution mapping of thick filaments' orientation in nonfibrilar muscle using polarization-sensitive second harmonic generation microscopy," J. Biomed. Opt. **14**(1), 014001 (2009).
18. F. Tiaho, G. Recher, and D. Rouède, "Estimation of helical angles of myosin and collagen by second harmonic generation imaging microscopy," Opt. Express **15**(19), 12286–12295 (2007).
19. S. Psilodimitrakopoulos, D. Artigas, G. Soria, I. Amat-Roldan, A. M. Planas, and P. Loza-Alvarez, "Quantitative discrimination between endogenous SHG sources in mammalian tissue, based on their polarization response," Opt. Express **17**(12), 10168–10176 (2009).
20. W.-L. Chen, T.-H. Li, P.-J. Su, C.-K. Chou, P. T. Fwu, and S.-J. Lin, "Second harmonic generation χ tensor microscopy for tissue imaging," Appl. Phys. Lett. **94**(18), 183902 (2009).
21. S. Psilodimitrakopoulos, V. Petegnief, G. Soria, I. Amat-Roldan, D. Artigas, A. M. Planas, and P. Loza-Alvarez, "Estimation of the effective orientation of the SHG source in primary cortical neurons," Opt. Express **17**(16), 14418–14425 (2009).
22. P. Réfrégier, M. Roche, and S. Brasselet, "Precision analysis in polarization-resolved second harmonic generation microscopy," Opt. Lett. **36**(11), 2149–2151 (2011).
23. S. Psilodimitrakopoulos, I. Amat-Roldan, P. Loza-Alvarez, and D. Artigas, "Effect of molecular organization on the image histograms of polarization SHG microscopy," Biomed. Opt. Express **3**(10), 2681–2693 (2012).
24. X. Han, R. M. Burke, M. L. Zettel, P. Tang, and E. B. Brown, "Second harmonic properties of tumor collagen: determining the structural relationship between reactive stroma and healthy stroma," Opt. Express **16**(3), 1846–1859 (2008).
25. M. Mathew, S. I. C. O. Santos, D. Zalvidea, and P. Loza-Alvarez, "Multimodal optical workstation for simultaneous linear, nonlinear microscopy and nanomanipulation: Upgrading a commercial confocal inverted microscope," Rev. Sci. Instrum. **80**(7), 073701 (2009).
26. S. Psilodimitrakopoulos, I. Amat-Roldan, P. Loza-Alvarez, and D. Artigas, "Estimating the helical pitch angle of amylopectin in starch using polarization second harmonic generation microscopy," J. Opt. **12**(8), 084007 (2010).
27. S. I. C. O. Santos, M. Mathew, O. E. Olarte, S. Psilodimitrakopoulos, and P. Loza-Alvarez, "Femtosecond laser axotomy in caenorhabditis elegans and collateral damage assessment using a combination of linear and nonlinear imaging techniques," PLoS One **8**(3), e58600 (2013).